Geophysical Research Letters

RESEARCH LETTER
10.1029/2018GL079429

Sources of Uncertainty in the Meridional Pattern of Climate Change

D. B. Bonan[1], **K. C. Armour**[1,2], **G. H. Roe**[3], **N. Siler**[4], **and N. Feldl**[5]

[1]Department of Atmospheric Sciences, University of Washington, Seattle, WA, USA, [2]School of Oceanography, University of Washington, Seattle, WA, USA, [3]Department of Earth and Space Sciences, University of Washington, Seattle, WA, USA, [4]College of Earth, Ocean, and Atmospheric Sciences, Oregon State University, Corvallis, OR, USA, [5]Department of Earth and Planetary Sciences, University of California, Santa Cruz, CA, USA

Key Points:
- A moist energy balance model explains approximately 90% of the variance in zonal mean surface warming of GCMs subject to CO_2 forcing
- Radiative feedbacks account for about 70% of the variance, with cloud feedbacks representing the largest source of uncertainty
- Tropical feedback uncertainty leads to warming uncertainty across all latitudes, whereas polar feedback uncertainty leads to warming uncertainty confined to the poles

Supporting Information:
- Supporting Information S1

Correspondence to:
D. B. Bonan,
dbonan@uw.edu

Citation:
Bonan, D. B., Armour, K. C., Roe, G. H., Siler, N., & Feldl, N. (2018). Sources of uncertainty in the meridional pattern of climate change. *Geophysical Research Letters*, *45*. https://doi.org/10.1029/2018GL079429

Received 30 JUN 2018
Accepted 4 AUG 2018
Accepted article online 22 AUG 2018

Abstract We employ a moist energy balance model (MEBM), representing atmospheric heat transport as the diffusion of near-surface moist static energy, to evaluate sources of uncertainty in the meridional pattern of surface warming. Given zonal mean patterns of radiative forcing, radiative feedbacks, and ocean heat uptake, the MEBM accurately predicts zonal mean warming as simulated by general circulation models under increased CO_2. Over a wide range of latitudes, the MEBM captures approximately 90% of the variance in zonal mean warming across the general circulation models, with approximately 70% of the variance attributable to differences in radiative feedbacks alone. Partitioning the radiative feedbacks into individual components shows that the majority of the uncertainty in the meridional pattern of warming arises from uncertainty in cloud feedbacks. Isolating feedback uncertainty within specific regions demonstrates that tropical feedback uncertainty leads to surface warming uncertainty that is global and nearly uniform with latitude, whereas polar feedback uncertainty leads to surface warming uncertainty that is largely confined to the poles.

Plain Language Summary In response to greenhouse gas forcing, global climate models—which physically describe how the climate system operates—predict a range of surface warming patterns. To better understand the sources of uncertainty in predicted warming patterns, we use an idealized climate model that links regional physical processes to warming responses across latitudes by representing changes in poleward atmospheric heat transport. We find that uncertainty in the spatial pattern of warming primarily arises from uncertainty in climate feedbacks, with uncertainty in climate forcing and ocean heat uptake playing smaller roles. Cloud feedbacks, in particular, contribute the greatest source of warming uncertainty in most regions. By considering the spread of climate feedbacks within distinct geographic regions, we show that feedback uncertainty in the tropics leads to warming uncertainty at all latitudes. However, feedback uncertainty in polar regions leads to warming uncertainty that is confined near the poles. The results suggest that polar warming is particularly difficult to predict because it is influenced by both local and nonlocal feedback processes. On the other hand, improved understanding of tropical cloud feedbacks has the potential to improve warming projections at all latitudes.

1. Introduction

Characterizing the relative importance of the sources of uncertainty in future climate change is a necessary step toward improving projections (e.g., Lovenduski & Bonan, 2017). Uncertainty arises from three distinct sources: internal climate variability, emissions scenario, and climate response (Hawkins & Sutton, 2009). Internal climate variability refers to natural fluctuations in climate that occur even in the absence of an external forcing. These fluctuations, intrinsic to the climate system, can mask the climate response to an external forcing (Deser et al., 2012). Uncertainty in emissions scenario arises primarily from our inability to predict future anthropogenic greenhouse gas emissions and land use changes (Raftery et al., 2017). Finally, comprehensive general circulation models (GCMs) have different representations of how the climate system behaves, producing divergent predictions of the climate response to greenhouse gas forcing.

A central goal of climate science is to understand how uncertainty in physical climate processes translate into uncertainty in the forced response (e.g., Roe, 2009). Considerable effort has gone toward quantifying sources of uncertainty in the equilibrium climate sensitivity (ECS), defined as the steady state global mean surface

temperature response to a doubling of CO_2. Studies show that a substantial portion of the intermodel spread in ECS results from how clouds are represented, with shortwave cloud feedbacks dominating the uncertainty in long-term warming (Andrews et al., 2012; Caldwell et al., 2016; Dufresne & Bony, 2008; Sherwood et al., 2014; Vial et al., 2013; Zhao et al., 2016). However, while ECS is an important quantity for intermodel comparison, its policy relevance is limited (Allen & Frame, 2007), given that it is a measure of the global mean, long-term climate response. Arguably, knowledge of the spatial pattern and transient evolution of climate change is of greater consequence for society.

A few key physical mechanisms govern the transient evolution of global mean climate. Radiative forcing, representing an externally imposed change in the Earth's top-of-atmosphere (TOA) radiation budget due to greenhouse gases or other forcing agents, drives changes in global surface temperature (e.g., Hansen et al., 1985). Radiative feedbacks, characterizing the TOA radiation response to surface warming (e.g., Bony et al., 2006; Roe, 2009; Roe & Baker, 2007), govern the long-term climate response to forcing. Finally, the uptake of heat by the ocean affects the rate of surface warming through the sequestration of energy at depth (e.g., Hansen et al., 1985; Raper et al., 2002). Due to the coupled nature of the climate system, assessing the relative contributions of these different mechanisms to projection uncertainty poses major challenges. Some diagnostic studies (e.g., Dufresne & Bony, 2008; Vial et al., 2013) suggest that shortwave cloud feedbacks are the primary source of uncertainty in the intermodel spread in the global mean climate response of GCMs, while others suggest that ocean heat uptake plays an important role, particularly for the early stages of transient warming (Boé et al., 2009). Yet such diagnostic studies lack the ability to evaluate the interactions among climate processes. Radiative response and ocean heat uptake, for instance, both contribute to global warming, but each also depends on the magnitude of warming itself (e.g., Raper et al., 2002). To overcome this limitation, Geoffroy et al. (2012) use a prognostic two-layer ocean model to quantify the sources of uncertainty in the global mean climate response across models as it evolves over time, permitting a quantification of the relative importance of different processes while preserving the interactions between them. They conclude the following: Uncertainty in the global mean response is primarily due to uncertainty in radiative feedbacks on long timescales, radiative forcing is a secondary source of uncertainty, and ocean heat uptake is an important source of uncertainty in the climate response for the first few decades but has little impact on the global temperature uncertainty thereafter—which is consistent with the results from Kostov et al. (2014).

Predicting the spatial pattern of climate change poses an even greater challenge than predicting the global mean. The fractional uncertainty in projected Arctic amplification, for instance, is more than a factor of 3 greater than that of the global mean warming (Graversen et al., 2008; Pithan & Mauritsen, 2014; Serreze et al., 2009). Recent studies have made progress in understanding the physical mechanisms responsible for robust spatial features of transient climate change, such as Arctic amplification (Holland & Bitz, 2003; Pithan & Mauritsen, 2014) and delayed Southern Ocean warming (Armour et al., 2016). The meridional pattern of surface warming is thought to depend on the structure of ocean heat uptake (Rose et al., 2014) and climate feedbacks (Roe et al., 2015) in particular. Yet an important question remains unanswered: What processes constitute the greatest sources of uncertainty in the meridional pattern of climate change? Previous studies have diagnosed the relative importance of different mechanisms within the response of fully coupled GCMs (e.g., Crook et al., 2011; Pithan & Mauritsen, 2014). Such diagnostic approaches, however, do not permit inference about how processes in one region affect the temperature response in another. Any accounting of sources of uncertainty in the spatial pattern of climate change must quantify the relative importance of interactions across latitudes.

In this study, we develop a framework for quantifying the sources of uncertainty in GCM projections of the meridional pattern of climate change based on a zonal mean moist energy balance model (MEBM). Given zonal mean patterns of radiative forcing, radiative feedbacks, and ocean heat uptake, the MEBM predicts the meridional pattern of surface warming by diffusing near-surface moist static energy down the meridional gradient, accounting for both sensible and latent heat changes. In what follows, we show that the MEBM is able to accurately capture the meridional patterns of warming as simulated by comprehensive GCMs subject to an abrupt quadrupling of CO_2. We then use the MEBM to evaluate the primary sources of uncertainty in both the magnitude and meridional pattern of surface warming, with a focus on characterizing how uncertainty in one part of the globe influences the climate response elsewhere.

2. Methods

2.1. Moist Energy Balance Model

Following Siler, Roe, and Armour (2018), we define $R_f(x)$ as the perturbation in TOA radiative forcing, as a function of sine latitude, x; $T(x)$ as the resulting change in near-surface air temperature; $\lambda(x)$ as the local net radiative feedback, defined as the TOA radiative response per degree of local surface warming ($W{\cdot}m^{-2}{\cdot}K^{-1}$; Armour et al., 2013; Feldl & Roe, 2013); $G(x)$ as the change in net surface heat fluxes (ocean heat uptake); and $\nabla \cdot F(x)$ as the change in the meridional divergence of the atmospheric heat transport. All quantities are defined as zonal and annual means. Conservation of energy connects these variables via the following:

$$G(x) = \lambda(x)T(x) + R_f(x) - \nabla \cdot F(x). \tag{1}$$

The MEBM solves for $T(x)$ using the assumption that $F(x)$ is proportional to the gradient of anomalous near-surface moist static energy, $h = c_pT + L_vq$, where c_p is the specific heat of air, L_v is the latent heat of vaporization, and q is the anomalous near-surface specific humidity. By convention, the relative humidity is fixed at 80%, making h a single-valued function of T. The simplest representation of downgradient transport is Fickian diffusion, which, on a sphere, is written as follows:

$$F = -\frac{2\pi p_s}{g} D(1-x^2)\frac{\mathrm{d}h}{\mathrm{d}x}, \tag{2}$$

where p_s is surface air pressure, g is the acceleration due to gravity, D is a constant diffusion coefficient (with units of m^2/s), and $(1 - x^2)$ accounts for the spherical geometry. Thus, the meridional divergence of the atmospheric heat transport is written as follows:

$$\nabla \cdot F(x) = -\frac{p_s}{a^2 g} D \frac{\mathrm{d}}{\mathrm{d}x}\left[(1-x^2)\frac{\mathrm{d}h}{\mathrm{d}x}\right], \tag{3}$$

where a is the radius of the Earth. We choose a value of D (9.6×10^5 m^2/s) that, given the zonal mean 2-m air temperature at sea level from the ERA-Interim Reanalysis (Dee et al., 2011), minimizes the mean square error between F calculated by equation (2) and northward atmospheric heat transport in ERA-Interim. The results from the following analysis, however, do not depend critically on the value of D. Combining (1) and (3) yields a single equation (the MEBM) that can be solved for $T(x)$, as a function of the spatial patterns of $R_f(x)$, $G(x)$, and $\lambda(x)$.

Building on an earlier idea proposed by Flannery (1984), the one-dimensional MEBM has proven to be remarkably successful at emulating the zonal mean climate response to radiative forcing and ocean heat uptake as simulated by comprehensive GCMs (Hwang & Frierson, 2010; Merlis & Henry, 2018; Roe et al., 2015; Rose et al., 2014; Siler, Roe, & Armour, 2018). These studies collectively suggest that, despite all of the complexities of atmospheric dynamics, many aspects of climate change can be understood as resulting from the atmosphere providing a downgradient transport of near-surface moist static energy (Roe et al., 2015).

2.2. CMIP5 Output

We use the MEBM to evaluate the sources of uncertainty in the meridional pattern of warming across 13 GCM experiments from phase 5 of the Coupled Model Intercomparison Project (CMIP5; Taylor et al., 2012). In particular, we consider the near-surface air temperature change centered 100 years after an abrupt quadrupling of atmospheric CO_2 above preindustrial levels. All the fields are the 31-year mean over years 85–115. The use of large radiative forcing, centennial timescale, and long (31-year) averaging period allows us to study the forced response of the GCMs. R_f is calculated from the change in TOA radiation in CO_2 quadrupling simulations performed with fixed preindustrial sea surface temperatures (Siler, Roe, Armour, & Feldl, 2018). G is calculated as the change in net surface heat fluxes within the fully coupled simulations. λ is calculated by equating the zonal mean net TOA radiation anomaly with $\lambda(x)T(x) + R_f(x)$. We further partition λ into individual feedback components (i.e., Planck, surface albedo, water vapor, lapse rate, and cloud feedbacks) using radiative kernels (see Feldl & Bordoni, 2016; Shell et al., 2008). The 13 GCMs used reflect all those that provided the necessary output for these calculations (see the supporting information for the list of models used).

Figure 1 shows R_f, G, and λ for each of the 13 GCMs used in this study, where the bold colored lines indicate the ensemble means. There are some common spatial patterns for R_f, G, and λ among the GCMs: R_f peaks in the tropics and diminishes toward the polar regions (Figure 1a); the largest absolute values of G are found in the Southern Ocean and North Atlantic Ocean, where ocean heat uptake is the largest due to regional ocean circulations (Armour et al., 2016; Marshall et al., 2015; Figure 1b); and there is a tendency for a more positive λ over the deep tropics and high latitudes (Figure 1c). Despite these commonalities, there is also considerable

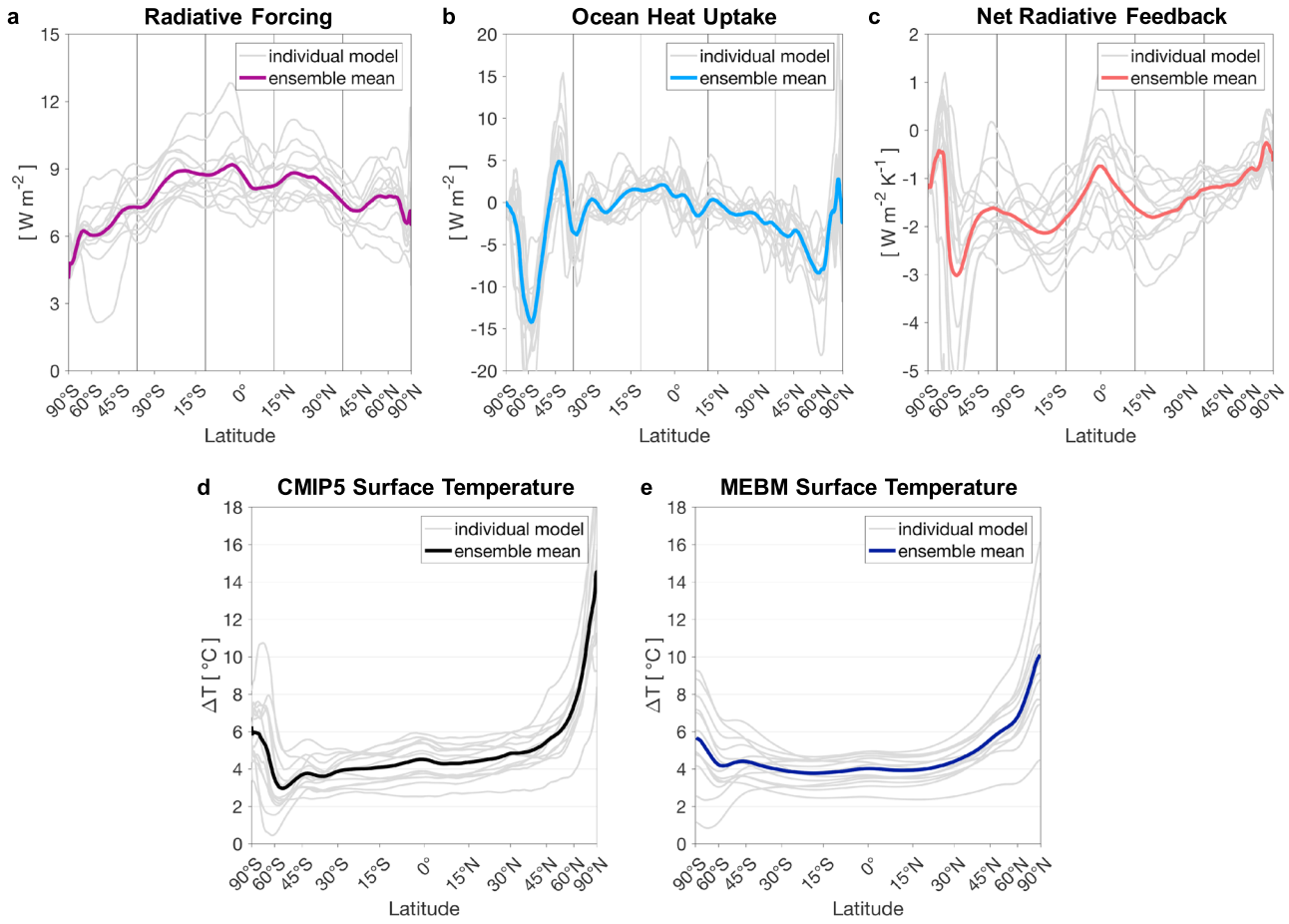

Figure 1. The zonal mean (a) radiative forcing (R_f), (b) ocean heat uptake (G), and (c) net radiative feedback (λ) for the 13 CMIP5 simulations 100 years after an abrupt CO_2 quadrupling. Negative values of G indicate heat uptake by the ocean. The zonal mean profile of surface warming 100 years after an abrupt CO_2 quadrupling for the (d) 13 CMIP5 general circulation models and (e) the corresponding MEBM solutions. The gray lines indicate individual models with each colored thick line being the ensemble mean. The vertical lines in (a)–(c) indicate the five equal-area regions. MEBM = moist energy balance model; CMIP5 = phase 5 of the Coupled Model Intercomparison Project.

spread in R_f, G, and λ across the GCMs. A key question is, how does the intermodel spread of each contribute to the spread in surface temperatures responses across the GCMs?

3. The MEBM and the CMIP5 Intermodel Spread

We first evaluate the ability of the MEBM to reproduce the temperature response of each GCM given its model-specific patterns of R_f, G, and λ and using (1) and (3) to solve for $T(x)$. Figure 1d shows $T(x)$ for each GCM, and Figure 1e shows $T(x)$ from the corresponding MEBM solution, where bold lines indicate ensemble means. The MEBM ensemble mean captures much of the large-scale structure of the GCM ensemble mean, including delayed Southern Ocean warming and Arctic amplification. Despite some discrepancies in the high latitudes of both hemispheres, the MEBM captures much of the intermodel variability in the meridional warming pattern. A quantitative assessment of the MEBM's skill is presented in Figure 2a through the black line. From 50°S to 60°N the MEBM captures 90 to 95% of the intermodel variability, with slightly less (70% to 80%) variance explained in the polar regions.

To better illustrate where the MEBM is skillful, we focus on five equal-area regions (delineated with black vertical lines in Figures 1a–1c). Although chosen for even spacing, each reflects a general region of the climate system: the middle-to-high latitudes (37°S to 90°S and 37°N to 90°N), the subtropics (12°S to 37°S and 12°N to 37°N), and the tropics (12°S to 12°N). We use two skill metrics for these regions: The variance in warming among the GCMs that the MEBM can explain and the root-mean-square error (RMSE), which quantifies the deviation of the MEBM solutions from the actual GCM responses (top left corners of Figures 2b–2f). From 37°S

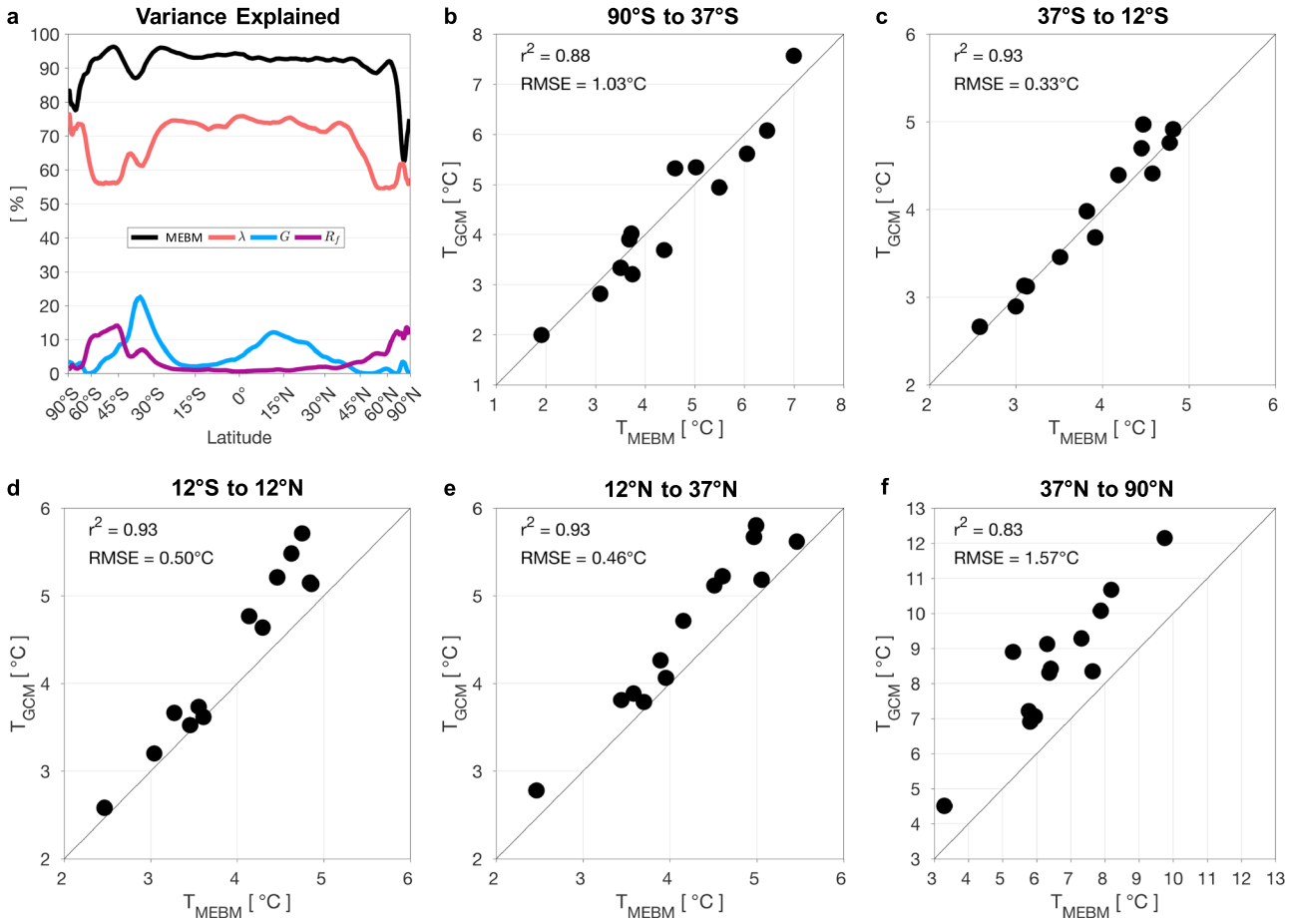

Figure 2. (a) The proportion of the variance (r^2), where r is the Pearson correlation coefficient, in the zonal mean GCM surface temperature response that is predictable from the zonal mean MEBM temperature solution as a function of latitude. The black line indicates result when using the GCM-specific patterns of R_f, G, and λ. The colored lines indicate the MEBM temperature solutions using the GCM-specific patterns of either λ (red line), G (blue line), or R_f (purple line) and the ensemble mean patterns of the others. (b–f) Scatter plots of the area-averaged GCM and MEBM temperature responses for each model in each of five equal-area regions (indicated by the gray vertical lines in Figures 1a–1c). The mean r^2 and RMSE values of each region are presented in the top left corner of each plot. RMSE = root-mean-square error; MEBM = moist energy balance model; GCM = general circulation model.

to 37°N (Figures 2c–2e), the MEBM captures the temperature response of the GCMs with high skill. On average in these regions, the MEBM solutions fall within 0.5°C of the actual GCMs and explain approximately 93% of the intermodel variance (Figures 2c–2e). In the middle-to-high latitudes of both hemispheres, the MEBM solutions deviate further from the GCM response and explain less intermodel variance. From 90°S to 37°S, the MEBM solutions fall within approximately 1°C of the GCM responses and explain about 88% of the intermodel variance (Figure 2b), whereas from 37°N to 90°N, the MEBM solutions underpredict the GCM temperature response by approximately 1.5°C on average and explain 83% of the intermodel variance (Figure 2f), falling to approximately 65% within the Arctic (Figure 2a). Overall, much of the intermodel spread in the zonal mean surface warming of GCMs can be explained given model-specific patterns of R_f, G, and λ.

4. Sources of Uncertainty

Having demonstrated that the MEBM accurately emulates the GCM temperature response for each individual model and the ensemble mean, we next evaluate what causes the intermodel spread of surface warming patterns. We disaggregate the temperature responses into separate contributions from R_f, G, and λ by creating a baseline set of patterns for the MEBM using the ensemble mean patterns of R_f, G, and λ. We then run the MEBM using the GCM-specific patterns of either R_f, G, or λ (Figures 1a–1c) while holding the other two variables fixed at their ensemble mean patterns. This generates a spread of MEBM temperature responses due to intermodel differences in either R_f, G, or λ.

The colored lines in Figure 2a show the degree to which uncertainty in each of R_f, G, and λ can explain the intermodel spread in the magnitude of the surface temperature response of the GCMs at each latitude. Note that since the MEBM is nonlinear, the individual contributions do not sum to the total variance explained when all variables are set to the GCM-specific patterns (i.e., the black line in Figure 2a). The analysis shows that the uncertainty in R_f (purple line) and G (blue line) explains at most about 20% of the spread in temperature responses at some latitudes and less in most other places. The contribution from G is largest (~20%) in the Southern Hemisphere midlatitudes where there is a large intermodel spread in ocean heat uptake (approximately 0 to 15 W/m^2; Figure 1b). Overwhelmingly, it is the spread in λ (red line; Figure 1c) that dominates uncertainty in the surface temperature response: Approximately 70% of the intermodel spread in surface temperature response is attributable to the intermodel spread of λ at most latitudes, although it falls to about 55% in the Southern Ocean and Arctic. These results suggest that radiative feedbacks are the primary source of uncertainty not only in global mean transient warming (Dufresne & Bony, 2008; Vial et al., 2013) but also in the meridional pattern of transient warming.

Another consideration is the extent to which radiative feedbacks contribute to the zonal mean warming through their impact on global mean warming. Indeed, warming across latitudes is highly correlated within both individual GCM and MEBM simulations (Figures 1d and 1e), reflecting the fact that different models produce relatively similar meridional structures of warming even with large differences in global mean warming (e.g., Leduc et al., 2016; Tebaldi & Arblaster, 2014). To evaluate what portion of the variance in zonal mean warming can still be explained when differences in global mean warming are accounted for, we normalize the response of the MEBM and each GCM by their respective global mean warming (Figure S1 in the supporting information). The MEBM is still able to explain approximately 60% of the intermodel spread in (normalized) surface warming throughout the tropics and midlatitudes and 80–90% of the intermodel spread in high latitudes. As before, the explained variance can be attributed primarily to the intermodel spread in λ, with G playing an important role at high latitudes. The large amount of variance explained by both λ and G, which add up to over 100% of the variance near the Southern Ocean, could be tied to their covariability (Po-Chedley et al., 2018). For the remainder of our analysis, we return to considering sources of uncertainty in the full pattern of warming (not normalized by global mean warming).

4.1. Individual Feedbacks

Having determined that the intermodel spread of λ is the main source of uncertainty in the meridional pattern of transient warming, we next consider the relative importance of individual feedbacks. We examine three groups of feedbacks calculated by radiative kernels (Feldl & Bordoni, 2016): the surface albedo feedback, the sum of the water vapor and lapse rate feedbacks, and the net (shortwave plus longwave) cloud feedback. To do this, we first remove the ensemble mean of each feedback group from the ensemble mean of λ and then add back in the GCM-specific patterns for each group — thus yielding an intermodel spread of each feedback group about the ensemble mean λ (Figures 3a–3c). We then run the MEBM with that spread in order to isolate the effects of uncertainty in each feedback group on the surface temperate response; in each case, G and R_f are fixed as ensemble mean patterns. The intermodel spread of the Planck feedback is not considered as it reduces to the temperature kernel and has little spread across models.

Figures 3d–3f show the ensemble mean, interquartile range, and full intermodel spread in warming due to the intermodel spread in each feedback group. The impact of uncertainty in the surface albedo feedback is largely confined to the polar regions (Figure 3d), contributing approximately 3 °C of warming uncertainty in the Arctic (full spread) and only about 1 °C of warming in the Antarctic (full spread). Relative to the surface albedo feedback, the intermodel spread in the combined lapse rate and water vapor feedbacks contributes comparable warming uncertainty in the Arctic (~3 °C) but greater warming uncertainty in the Antarctic (~2.5 °C). Notably, the combined spread of the lapse rate and water vapor feedbacks is not confined to any specific region; uncertainty is distributed quite evenly across latitudes. It is the intermodel spread in the net cloud feedback that contributes the most warming uncertainty at all latitudes: ~7 °C of warming uncertainty in the Arctic and ~4 °C in the tropics and Antarctic. Note that the warming uncertainty induced by each feedback group does not add up to the total warming uncertainty induced by λ, owing to the nonlinearity of the warming response to feedback uncertainty (Roe, 2009).

4.2. Local Versus Nonlocal Uncertainty

Another feature of the above results is that warming uncertainty is not generally confined to the same latitudes of greatest feedback uncertainty. For instance, the intermodel spread of cloud feedbacks is largest in

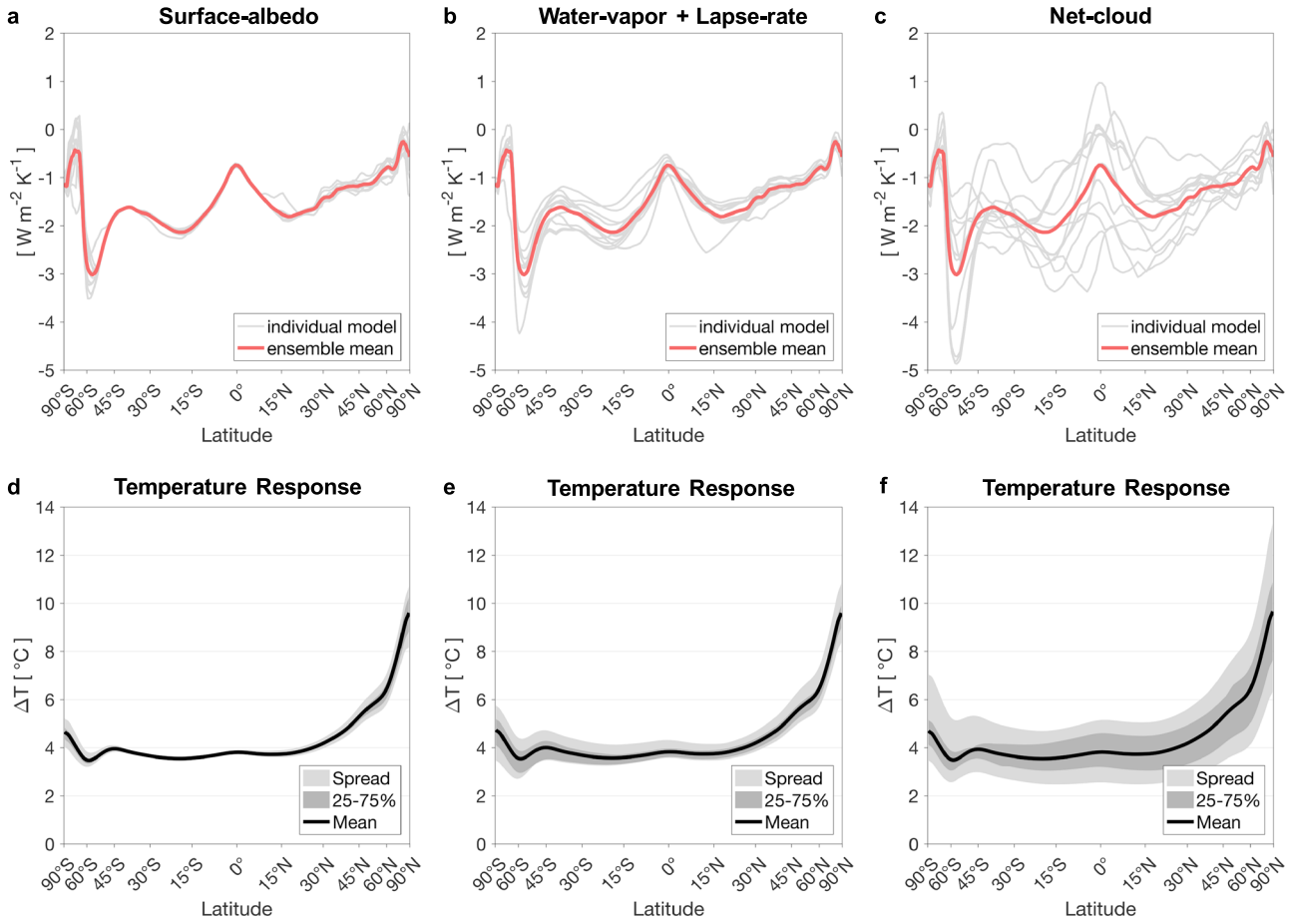

Figure 3. Zonal mean λ (red line) with the model-specific patterns (gray lines) of (a) the surface albedo feedback, (b) combined water vapor and lapse rate feedbacks, and (c) shortwave and longwave cloud feedbacks. The zonal mean MEBM temperature response due to the intermodel spread of (d) the surface albedo feedbacks, (e) combined water vapor and lapse rate feedbacks, and (f) shortwave and longwave cloud feedbacks. The ensemble mean patterns of G and R_f were used for these MEBM temperature solutions. With the temperature responses, the black lines indicate the ensemble mean, the dark gray shading is the 25% to 75% percentiles, and the light gray shading is the full spread of the models. MEBM = moist energy balance model.

the tropics (Figure 3c), yet the associated warming uncertainty is distributed nearly uniformly across latitudes (Figure 3f). This suggests that characterizing the sources of uncertainty in zonal mean warming requires an understanding of how the local response depends on nonlocal climate processes. To highlight the local versus nonlocal nature of uncertainty in the meridional pattern of transient warming, we next run the MEBM with GCM-specific values of λ applied within individual equal-area regions only (see section 3) while holding λ at all other latitudes fixed at the ensemble mean value. For each analysis, G and R_f are set to the ensemble mean pattern. This yields a spread of temperature responses at all latitudes due to the local spread of λ in particular regions.

Figure 4 shows the ensemble mean, interquartile range, and full intermodel spread in T due to the intermodel spread in λ for each of the five equal-area regions. For the spread of λ in the tropics, uncertainty in T is nearly uniform with latitude, adding more than 1 °C of warming uncertainty (full spread) across the globe (Figure 4a). Feedback uncertainty in the northern subtropics (Figure 4c) has a larger impact in northern high latitudes (~2 °C) than locally (~1.25 °C). Finally, feedback uncertainty at the middle-to-high latitudes causes large uncertainty in local T and strongly diminished impact elsewhere (Figures 4d and 4e). The local spread of λ adds approximately 3 °C of warming uncertainty in the middle-to-high latitudes of the Northern Hemisphere and about 5 °C of warming uncertainty in the middle-to-high latitudes of the Southern Hemisphere.

The above findings reflect the strong tendency of atmospheric circulations to redistribute energy downgradient and so, too, the tendency to preferentially redistribute uncertainty poleward (Roe et al., 2015). The result is that uncertainty in high-latitude feedbacks results in warming uncertainty that is largely confined to the

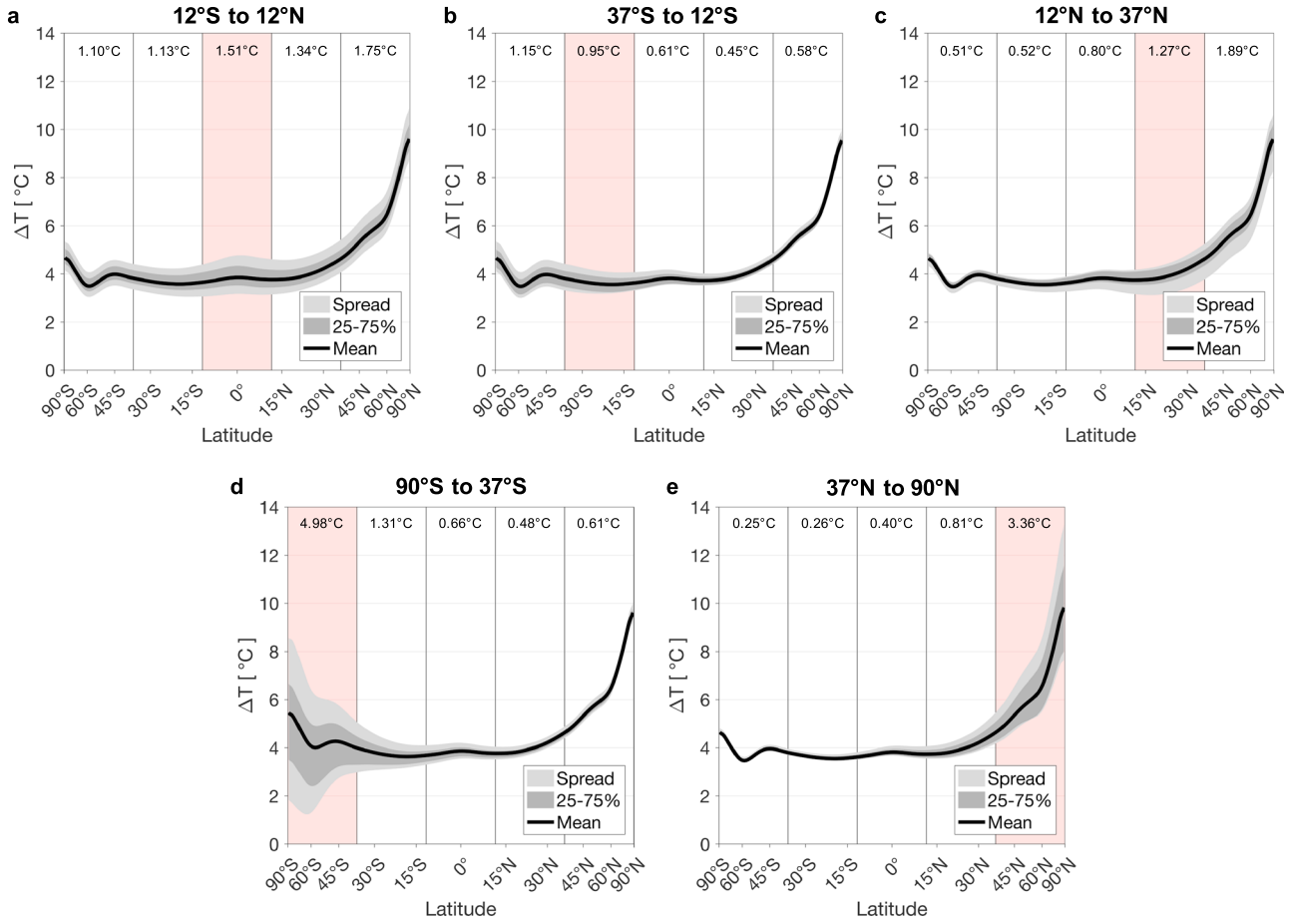

Figure 4. The zonal mean moist energy balance model surface temperature response with the ensemble mean G, ensemble mean R_f, and intermodel spread of λ in (a) the tropics (12°S to 12°N), (b) Southern Hemisphere subtropics (12°S to 37°S), (c) Northern Hemisphere subtropics (12°N to 37°N), (d) Southern Hemisphere middle-to-high latitudes (37°S to 90°S), and (e) Northern Hemisphere middle-to-high latitudes (37°N to 90°N). The black lines indicate the ensemble mean, the dark gray shading is the 25th to 75th percentiles, and the light gray shading is the full spread of the models. The red-shaded area is the region where the intermodel spread of λ was applied, and the white regions are where λ is set to the ensemble mean values. The numbers over each region indicate the full intermodel spread of surface temperature responses induced both locally and nonlocally by feedback variations in the red-shaded region.

high latitudes, while uncertainty in low-latitude feedbacks results in warming uncertainty that is distributed uniformly. These results provide physical intuition for why projected warming is most uncertain at the poles: Uncertainties in nonlocal processes affect polar warming uncertainty, and thus constraining polar warming requires constraining climate processes everywhere — not just in polar regions. Meanwhile, constraining polar feedbacks does little to constrain tropical warming, which depends primarily on tropical processes.

5. Discussion and Conclusion

Comprehensive climate models diverge in their projections of future climate change, particularly at regional scales. The enormous complexity of GCMs, however, hinders our ability to evaluate the relative importance of the different factors driving that uncertainty. Rather than using GCMs directly, here we evaluated the primary sources of uncertainty in the meridional pattern of transient warming by using an idealized zonal mean energy balance model that assumes a downgradient transport of moist static energy (the MEBM).

Figures 1 and 2 demonstrate the ability of the MEBM to accurately capture the zonal mean surface warming of an ensemble of comprehensive GCMs in response to an abrupt quadrupling of CO_2 above preindustrial levels. Over a wide range of latitudes, the MEBM captures approximately 90% of the intermodel variability in surface warming. In the Arctic, however, the MEBM captures less of the intermodel variability and shows a bias toward too little warming. Nonetheless, these results suggest that overall the MEBM is a useful tool for studying the intermodel variations of climate projections. Recent work demonstrates that the MEBM emulates

modeled changes to the zonal mean hydrological cycle and provides a novel perspective on the expansion of the subtropics and the poleward migration of the storm tracks (Siler, Roe, & Armour, 2018). The MEBM could also be used to deconstruct the climate response to other forcings such as anthropogenic and volcanic aerosols, solar variability, and orbital variations. Such an analysis could provide valuable information about the relative roles of the pattern of aerosol radiative forcing versus the pattern of ocean heat uptake induced by that aerosol forcing (Shi et al., 2018; Wang et al., 2016) on the meridional pattern of warming.

By applying the intermodel variations of R_f, G, and λ independently, we find that uncertainty in the meridional pattern of transient warming is dominated by the intermodel spread of λ (Figure 2a). By further partitioning λ into individual feedbacks, we identified cloud feedbacks as the largest source of uncertainty in the meridional pattern of transient warming (Figure 3f). Uncertainty in the combined spread of the lapse rate and water vapor feedbacks leads to global uncertainty in the surface temperature response (Figure 3e), while the intermodel spread of the surface albedo feedback contributes to warming uncertainty of the polar regions (Figure 3d). Our analyses of the impact of feedback uncertainty in specific regions illustrate how physical processes in one part of the globe can influence the climate response elsewhere. The intermodel spread of λ in the tropics and midlatitudes leads to warming uncertainty that is global and nearly uniform (Figures 4a–4c), while the intermodel spread of λ in the polar regions leads to warming uncertainty that is largely confined largely to the poles (Figures 4d and 4e). A potential caveat to this decomposition is that the magnitude of ocean heat uptake—treated as a forcing within the MEBM—may depend to some extent on the pattern of warming and feedbacks themselves. An illustration of the potential impact of regional uncertainties in ocean heat uptake and forcing is provide in the supporting information through the same equal-area analysis for uncertainties in G and R_f. Uncertainty in G at the high latitudes projects large amounts of warming uncertainty in the high latitudes (Figure S2). A useful extension of this line of research would be to evaluate the sources of warming uncertainty within a version of the MEBM coupled to a dynamic ocean, as the relative importance of ocean heat uptake on warming uncertainty may increase.

Our results suggest that uncertainty in polar regions is the aggregate of both local and nonlocal feedback uncertainty. Uncertainty in Arctic amplification is largely the result of strong local feedbacks that amplify uncertainty from all sources. Uncertainty in the lapse rate and water vapor feedbacks combined contributes a similar amount of warming uncertainty to the poles as the spread of the surface albedo feedbacks, while cloud feedbacks contribute an even greater amount of polar warming uncertainty. Much of this polar warming uncertainty arises through feedback uncertainty that is from the tropics and midlatitudes. These results suggest that the atmosphere acts to preferentially spread uncertainty in response poleward—down the moist static energy gradient. Thus, uncertainty in cloud feedbacks, from any region, projects large amounts of warming uncertainty in the polar regions. To develop confidence in model projections of future warming of the polar regions, it is thus necessary to constrain not only polar processes but also nonlocal processes.

As GCMs reach higher levels of sophistication, and the number of parameterizations increase, it becomes ever more difficult to attribute model response to specific factors, such as radiative feedbacks. The ability of the MEBM to emulate the behavior of comprehensive GCMs indicates its advantage in evaluating how uncertainties in these patterns are redistributed in latitude via downgradient energy transport. Key implications of this work are that reducing uncertainty in climate projections requires improved understanding of radiative feedbacks—particularly those associated with clouds in the tropics, which will improve projections over a wide range of latitudes. Meanwhile, improved understanding of polar feedbacks will primarily reduce warming uncertainty in polar regions.

Acknowledgments
D. B. B. was supported by a research grant under the University of Washington Mary Gates Endowment for Undergraduate Students. K. C. A. was supported by NSF grant AGS-1752796. N. F. was supported by NSF grant AGS-1753034. The CMIP5 data for this study are accessible at the Earth System Grid Federation (ESGF) Portal (https://esgf-node.llnl.gov/search/cmip5/).

References

Allen, M. R., & Frame, D. J. (2007). Call off the quest. *Science*, *318*(5850), 582–583.

Andrews, T., Gregory, J. M., Webb, M. J., & Taylor, K. E (2012). Forcing, feedbacks and climate sensitivity in CMIP5 coupled atmosphere-ocean climate models. *Geophysical Research Letters*, *39*, L09712. https://doi.org/10.1029/2012GL051607

Armour, K. C., Bitz, C. M., & Roe, G. H. (2013). Time-varying climate sensitivity from regional feedbacks. *Journal of Climate*, *26*(13), 4518–4534.

Armour, K. C, Marshall, J., Scott, J. R., Donohoe, A., & Newsom, E. R (2016). Southern ocean warming delayed by circumpolar upwelling and equatorward transport. *Nature Geoscience*, *9*(7), 549.

Boé, J., Hall, A., & Qu, X. (2009). Deep ocean heat uptake as a major source of spread in transient climate change simulations. *Geophysical Research Letters*, *36*, L22701. https://doi.org/10.1029/2009GL040845

Bony, S., Colman, R., Kattsov, V. M., Allan, R. P., Bretherton, C. S., Dufresne, J.-L., et al. (2006). How well do we understand and evaluate climate change feedback processes? *Journal of Climate*, *19*(15), 3445–3482.

Caldwell, P. M., Zelinka, M. D., Taylor, K. E., & Marvel, K. (2016). Quantifying the sources of intermodel spread in equilibrium climate sensitivity. *Journal of Climate*, *29*(2), 513–524.

Crook, J. A., Forster, P. M., & Stuber, N. (2011). Spatial patterns of modeled climate feedback and contributions to temperature response and polar amplification. *Journal of Climate*, *24*(14), 3575–3592.
Dee, D. P., Uppala, S. M., Simmons, A. J., Berrisford, P., Poli, P., Kobayashi, S., et al. (2011). The ERA-Interim reanalysis: Configuration and performance of the data assimilation system. *Quarterly Journal of the royal meteorological society*, *137*(656), 553–597.
Deser, C., Phillips, A., Bourdette, V., & Teng, H. (2012). Uncertainty in climate change projections: The role of internal variability. *Climate dynamics*, *38*(3-4), 527–546.
Dufresne, J.-L., & Bony, S. (2008). An assessment of the primary sources of spread of global warming estimates from coupled atmosphere–ocean models. *Journal of Climate*, *21*(19), 5135–5144.
Feldl, N., & Bordoni, S. (2016). Characterizing the Hadley circulation response through regional climate feedbacks. *Journal of Climate*, *29*(2), 613–622.
Feldl, N., & Roe, G. (2013). Four perspectives on climate feedbacks. *Geophysical Research Letters*, *40*, 4007–4011. https://doi.org/10.1002/grl.50711
Flannery, B. P. (1984). Energy balance models incorporating transport of thermal and latent energy. *Journal of the Atmospheric Sciences*, *41*(3), 414–421.
Geoffroy, O., Saint-Martin, D., & Ribes, A. (2012). Quantifying the sources of spread in climate change experiments. *Geophysical Research Letters*, *39*, L24703. https://doi.org/10.1029/2012GL054172
Graversen, R. G., Mauritsen, T., Tjernström, M., Källén, E., & Svensson, G. (2008). Vertical structure of recent Arctic warming. *Nature*, *451*(7174), 53.
Hansen, J., Russell, G., Lacis, A., Fung, I., Rind, D., & Stone, P. (1985). Climate response times: Dependence on climate sensitivity and ocean mixing. *Science*, *229*(4716), 857–859.
Hawkins, E., & Sutton, R. (2009). The potential to narrow uncertainty in regional climate predictions. *Bulletin of the American Meteorological Society*, *90*(8), 1095–1107.
Holland, M. M., & Bitz, C. M. (2003). Polar amplification of climate change in coupled models. *Climate Dynamics*, *21*(3–4), 221–232.
Hwang, Y.-T., & Frierson, D. M. (2010). Increasing atmospheric poleward energy transport with global warming. *Geophysical Research Letters*, *37*, L24807. https://doi.org/10.1029/2010GL045440
Kostov, Y., Armour, K. C., & Marshall, J. (2014). Impact of the Atlantic meridional overturning circulation on ocean heat storage and transient climate change. *Geophysical Research Letters*, *41*, 2108–2116. https://doi.org/10.1002/2013GL058998
Leduc, M., Matthews, H. D., & de Elía, R. (2016). Regional estimates of the transient climate response to cumulative CO_2 emissions. *Nature Climate Change*, *6*(5), 474.
Lovenduski, N. S., & Bonan, G. B. (2017). Reducing uncertainty in projections of terrestrial carbon uptake. *Environmental Research Letters*, *12*(4), 044020.
Marshall, J., Scott, J. R., Armour, K. C., Campin, J.-M., Kelley, M., & Romanou, A. (2015). The ocean's role in the transient response of climate to abrupt greenhouse gas forcing. *Climate Dynamics*, *44*(7-8), 2287–2299.
Merlis, T. M., & Henry, M. (2018). Simple estimates of polar amplification in moist diffusive energy balance models. *Journal of Climate*, *31*, 5811–5824. https://doi.org/10.1175JCLI-D-17-0578.1
Pithan, F., & Mauritsen, T. (2014). Arctic amplification dominated by temperature feedbacks in contemporary climate models. *Nature Geoscience*, *7*(3), 181.
Po-Chedley, S., Armour, K. C., Bitz, C. M, Zelinka, M. D., Santer, B. D., & Fu, Q. (2018). Sources of intermodel spread in the lapse rate and water vapor feedbacks. *Journal of Climate*, *31*(8), 3187–3206.
Raftery, A. E., Zimmer, A., Frierson, D. M., Startz, R., & Liu, P. (2017). Less than 2 °C warming by 2100 unlikely. *Nature Climate Change*, *7*(9), 637.
Raper, S. C., Gregory, J. M., & Stouffer, R. J. (2002). The role of climate sensitivity and ocean heat uptake on AOGCM transient temperature response. *Journal of Climate*, *15*(1), 124–130.
Roe, G. (2009). Feedbacks, timescales, and seeing red. *Annual Review of Earth and Planetary Sciences*, *37*, 93–115.
Roe, G. H., & Baker, M. B. (2007). Why is climate sensitivity so unpredictable? *Science*, *318*(5850), 629–632.
Roe, G. H., Feldl, N., Armour, K. C., Hwang, Y.-T., & Frierson, D. M. (2015). The remote impacts of climate feedbacks on regional climate predictability. *Nature Geoscience*, *8*(2), 135–139.
Rose, B. E., Armour, K. C., Battisti, D. S., Feldl, N., & Koll, D. D. (2014). The dependence of transient climate sensitivity and radiative feedbacks on the spatial pattern of ocean heat uptake. *Geophysical Research Letters*, *41*, 1071–1078. https://doi.org/10.1002/2013GL058955
Serreze, M. C., Barrett, A. P., Stroeve, J. C., Kindig, D. N., & Holland, M. M. (2009). The emergence of surface-based arctic amplification. *The Cryosphere*, *3*(1), 11–19.
Shell, K. M., Kiehl, J. T., & Shields, C. A. (2008). Using the radiative kernel technique to calculate climate feedbacks in NCAR's community atmospheric model. *Journal of Climate*, *21*(10), 2269–2282.
Sherwood, S. C., Bony, S., & Dufresne, J.-L. (2014). Spread in model climate sensitivity traced to atmospheric convective mixing. *Nature*, *505*(7481), 37–42.
Shi, J. R., Xie, S. P., & Talley, L. D. (2018). Evolving Relative Importance of the Southern Ocean and North Atlantic in Anthropogenic Ocean Heat Uptake. *Journal of Climate*, *31*(18), 7459–7479.
Siler, N., Roe, G. H., & Armour, K. C. (2018). Insights into the zonal-mean response of the hydrologic cycle to global warming from a diffusive energy balance model. *Journal of Climate*, *31*(18), 7481–7493. https://doi.org/10.1175/JCLI-D-18-0081.1
Siler, N., Roe, G. H., Armour, K. C., & Feldl, N. (2018). Revisiting the surface-energy-flux perspective on the sensitivity of global precipitation to climate change. *Climate Dynamics*, 1–13. https://doi.org/10.1007/s00382-018-4359-0
Taylor, K. E., Stouffer, R. J., & Meehl, G. A. (2012). An overview of CMIP5 and the experiment design. *Bulletin of the American Meteorological Society*, *93*(4), 485–498.
Tebaldi, C., & Arblaster, J. M. (2014). Pattern scaling: Its strengths and limitations, and an update on the latest model simulations. *Climatic Change*, *122*(3), 459–471.
Vial, J., Dufresne, J.-L., & Bony, S. (2013). On the interpretation of inter-model spread in CMIP5 climate sensitivity estimates. *Climate Dynamics*, *41*(11-12), 3339–3362.
Wang, H., Xie, S.-P., & Liu, Q. (2016). Comparison of climate response to anthropogenic aerosol versus greenhouse gas forcing: Distinct patterns. *Journal of Climate*, *29*(14), 5175–5188.
Zhao, M., Golaz, J.-C., Held, I. M., Ramaswamy, V., Lin, S.-J., Ming, Y., et al. (2016). Uncertainty in model climate sensitivity traced to representations of cumulus precipitation microphysics. *Journal of Climate*, *29*(2), 543–560.